Electronic and Magnetic Properties of $FeWO_4$ Nanostructures Synthesized by Microwave Assisted Hydrothermal Method

M. A. P. Almeida [a*], C. Morilla-Santos [c], L. S. Cavalcante [b], P. N. Lisboa Filho[c], A. Beltrán[d], J. Andrés,[d] L. Gracia[d], E. Longo[a,b], J. A. Varela[b]

[a] *INCTMN-DQ-Universidade Federal de São Carlos, São Carlos, P.O. Box 676, 13565-905, SP, Brazil*

[b] *INCTMN -Universidade Estadual, Paulista, P.O. Box 355, 14801-907, Araraquara, SP, Brazil*

[c] *MAv -Universidade Estadual, Paulista, P.O. Box 473, 17033-360, Bauru, SP, Brazil*

[d] *Department de Química Física i Analítica, Universitat Jaume I, E-12071 Castelló, Spain*

Abstract

$FeWO_4$ nanostructures were successfully synthesized by a microwave assisted hydrothermal method. The structure and morphology of nanocrystals were characterized by Rietveld refinement of XRD, TEM, and HRTEM images. Combining the experimental findings, first principles calculations are used to investigate the electronic and magnetic properties.

On the basis of the results obtained by magnetization measurements.for different applied magnetic fields and first-principles calculations, we find that the main magnetic properties of $FeWO_4$ nanostructures can be assigned to the presence of two magnetic orderings with parallel or antiparallel spins in adjacent chains that are the key to understand the competition between the ferro- and antiferro- magnetic behavior.

Metal tungstates have attracted attention in the last decades since they are a fascinating class of materials that offer a large wide of technological applications, such as catalysts,[1] optics,[2] humidity sensors,[3] and magnetic,[1,4,5,6] properties. Iron tungstate ($FeWO_4$) is one of the most promising materials of this family and their electronic and magnetic properties have been studied to explore its potential applications.[1,4,7]

The electronic and magnetic structures of $FeWO_4$ have been scarcely studied and further studies on magnetic behavior in $FeWO_4$ are necessary to deep understand their fundamental properties. Recently, Stüβer *et al.*[8] and Rajagopal *et al.*[9] reported some magnetic properties of $FeWO_4$ and others isomorphous transition-metal tungstates systems such as $MnWO_4$, $NiWO_4$, $CoWO_4$ indicating that these systems have an incomplete 3d shell and are paramagnetic at room temperature, while at low temperatures, these complex metal oxides undergo cooperative transitions to antiferromagnetically ordered states.[10]

One of the main difficulties to study transition-metal tungstates is related to obtaining high quality single phase samples. Numerous synthetic procedures for obtaining $FeWO_4$ have been developed such as the conventional solid-state, the spray pyrolysis, the Czochralski method, and the hydrothermal route, among others.[1,2,5,7,11-13] However, these procedures require long processing times and some of them high temperatures; therefore, it remains a great challenge to develop a feasible method for the synthesis of $FeWO_4$ nanostructures. To lower the time requirements and the temperature of the synthesis, microwave assisted hydrothermal (MAH) has been used in recent years and it is one of the most promising methods for the preparation of nanomaterials with controlled size and shape.[14] The MAH processing is fast, clean, simple and often energetically more efficient than conventional heating. Our group has been used MAH method to obtain tailor-

made nanostructures of different metal oxides,[15] showing it is quite efficient because it is possible to synthetize nanocrystalline materials in short reduced times, mild processing temperatures, and use of environmentally friendly solvents. In addition, this method possesses the capabilities of time and temperature programming, allowing fast and easy optimization of experimental factors.[15] This is very beneficial for creating numerous synthetic recipes, preparing high-quality nanomaterials, and scaling up production. According to our knowledge such an approach has not been applied to obtain to the investigated system so far.

In this letter, we report the synthesis of $FeWO_4$ nanostructures by the use of MAH method, with narrow size distribution, and high density of surface area, which are suitable for technological applications. The as-synthesized $FeWO_4$ nanostructures were characterized by X-ray diffraction (XRD), and transmission electron microscopy (TEM) and high resolution (HRTEM), and the corresponding selected-area electron diffraction (SAED) pattern were captured. An understanding of the electronic and magnetic properties has been achieved by a combination of first principle calculations and experimental measurements.

The typical procedure for the synthesis of $FeWO_4$ nanostructures was as follows. A solution containing 10 mmol (0.33 g) of sodium tungstate and 20 mmol (0.57 g) of sodium dodecil sulphate (SDS) followed by the addition of 10 mmols (0.39 g to iron) of iron sulfate [$(NH_4)_2Fe(SO_4)_2.6H_2O$, 99.99% purity, Aldrich] were dissolved, while the pH=9 was maintained with NH_4OH before processing. In the sequence, this suspension was transferred into a Teflon autoclave which was sealed and placed inside a domestic microwave system and processed at 443 K for 45 min.

Magnetization versus applied magnetic field in zero field cooled (ZFC) and field cooled (FC) measurements were performed using a Quantum Design Magnetic Properties Measurement System (MPMS) XL-5 Superconducting Quantum Interference Device..

Structural and geometrical parameters, obtained from the Rietveld refinement of XRD,[16] are shown in Table 1. All the detectable peaks in the XRD pattern can be assigned to a monoclinic structure belonging to the P2/c space group, with unit cell parameters, a = 4.6800 Å, b = 5.6975 Å, c = 4.9841 Å, β = 89.881º (JPCDS card file Nº 71-2390), see Figure 1(a). No secondary phases were detected, demonstrating that the products are very high-purity and single phase. In addition, the intense and sharp diffraction peaks suggest that the as-synthesized products have a high degree of crystallization. An analysis and comparison of these data point out that the corresponding values are consistent with the reported values of Rajagopal et al.[11], and previous value reported by others.[1,13,17]

In the structure of $FeWO_4$ with two formulas per unit cell, every metal atom is surrounded by six oxygen atoms, FeO_6 and WO_6; zigzag chains of oxygen octahedral FeO_6 are aligned along the c axis, see Figure 1(a). The existence of two non-equivalent positions for oxygen atoms is a characteristic of the structure of $FeWO_4$. There are two W atoms and one Fe atom in the nearest arrangement of the O1 atoms, whilst one W atom and two iron atoms are among the nearest neighbors of the O2 atoms.

(Table 1)

(Fig. 1)

First-principles-based density functional theory (DFT) calculations for semi-quantitative determination is commonly used to deeper understand the crystal structure and its relation to the magnetic (spin density) and electronic (band gap and density of states) properties of this material**.** Here we combine insights from DFT simulations, with atomic

positions and unit cell parameters. All the calculations have been carried out with the CRYSTAL 09 program,[18] in the framework of the DFT with the hybrid functional B3LYP.[19] Fe, W and O centers have been described in the scheme 86-411d41G, [PS] -11d31G and 8-411G, respectively, where [PS] stands for the effective core potential. The definition of core and valence electrons for the valence basis set representing the Fe, W and O centers can be found at CRYSTAL web site.[20]

In order to understand the magnetic behavior of $FeWO_4$ system, we have employed the periodic supercell technique, by using 2x1x1 unit cell doubled along *a* direction. This model comprises four Fe atoms with a $3d^6$ electronic configuration. According to our knowledge such an approach has not been applied to the investigated system so far. We have explored three different spin states for each of the four Fe atoms, i.e. high spin (quintuplet), low spin (triplet) and closed shell (singlet), being the high spin state the most stable. The calculations have been performed for four magnetic states by fixing the total spin S. The first state is associated to antiferromagnetic state (AF1) with the ferromagnetic ordering of spins at Fe atoms within zigzag chains but the antiferromagnetic alignment between adjacent chains (see Fig. 1a).

Note that AF1 state requires the doubling of crystallographic unit cell along a-axis direction. There is also another possibility for AF state (AF2) with S = 0 when spins at Fe ions in the same chain have antiparallel arrangement: in this case, no cell doubling is required since there are two Fe ions per primitive cell. The ferromagnetic (FM) state with all spins at Fe atoms ordered collinearly and the non-magnetic (NM) state has also been calculated.

The AF1 is the most stable state where Fe atoms belonging to adjacent chains interact antiferromagnetically at a distance of 4.68 Å along *a* direction. AF1 lies 1.1, 1.6 and 11.4

eV lower in energy than FM, AF2 and NM states, respectively. For AF1, the calculations render that the magnetic moment on each Fe atom is 3.65 μ_B (~4 μ_B). The Mulliken population analysis was used to estimate the total atomic charges. They are equal to +1.73e for Fe, +3.18e for W, -1.02e for O1, and -1.24e for O2. These values point out that both Fe-O and W-O bonds have a mixed ionic-covalent character. The value around +3 for W, instead of +6 for the purely ionic, indicates the presence of a back charge transfer process from the nearest oxygen atom, O1 and O2. This process is responsible for the strong distortion of the WO_6 octahedra associated to a second-order Jahn-Teller Effect.[21] As result, there are three different lengths for both W-O bonds (W-O2: 1.70 Å, W-O1: 1.97 Å, and W-O1: 2.28 Å) and Fe-O bonds (Fe-O1: 1.86 Å, Fe-O2: 2.16 Å, and Fe-O2: 2.23 Å)

Fig. 1(b) shows the projected spin density map for the most stable AF1 configuration. An analysis of the results shows that the Fe atoms belonging to adjacent chains present α and β spin density distributions. The O and W atoms closer to these Fe atoms are affected in a very symmetric way in such a manner that the final magnetic response is zero.

Figure 2(a) shows the TEM images of $FeWO_4$ nanostructures. It is possible to verify that the nanostructures have various sizes ranging from 10 nm to 50 nm. An analysis of the results renders that these nanoparticles have grown by an oriented attachment process, in which the large nanostructures are formed from the adjacent nanostructures, having a preferential [110] growth direction. The HRTEM image for $FeWO_4$ of Figure 2(b) shows lattice distances of 0.36 and 0.47 nm, that correspond to the interplanar spacing of the (110) and (100) planes, respectively, of the monoclinic $FeWO_4$ structure. In Figure 2(b) the SAED pattern takes along the [100] zone axis from whole $FeWO_4$ nanostructures that was indexed as a polycrystalline $FeWO_4$ phase.

(Fig. 2)

The thermal variation of magnetizations measured for different applied magnetic fields for ZFC and FC are depicted in Figure 3. An analysis of the curves shows that both FM and AF components coexist at low temperatures.

(Fig.3)

The temperature dependence of the magnetization, measured at 10 Oe, 100Oe, 1 KOe and 10 KOe, shows an irreversible behavior between the ZFC and FC curves. Another important feature should be pointed out, concerning the presence of a shoulder followed by a pronounced slope of the ZFC magnetization between 2 and 50 K at 10 Oe, 100 Oe and 1 KOe. The main contribution of the antiferromagnetic component with a Néel critical temperature T_N close to 54 K drastically decreases as the magnetic field increases at 10 KOe and is suppressed at 50 KOe. This value of T_N is much lower than previously reported elsewhere.[1,7] Otherwise, at lower temperatures, a weaker ferromagnetism can also be observed due to inner chains.

Using the experimental geometry we obtain an indirect bandgap from Γ (0,0,0) to A (½,½,0) of 1.65 eV, being the direct gap at Γ of 1.76 eV. This value is similar to that of 1.78 eV found by Rajagopal *et al*[9] using FP-LAPW calculations. To further illustrate the origin behind magnetism in the $FeWO_4$, the analysis of the band structure and partial density of states points out that the upper valence band is constituted mainly by the Fe 3d orbitals (mostly d_{xy} and d_{yz}) and in less extension by the O 2p orbitals with a very little contribution of the W 5d orbitals. The predominant contribution into the lower region of the conduction band is due to the W 5d states, the O 2p and the Fe 3d orbitals in minor extent.

In summary, $FeWO_4$ nanocrystals were synthesized by the MAH method. These nanocrystals were characterized by XRD, TEM, and HRTEM measurements. On the basis of first-principles calculations and temperature dependence measures for different applied magnetic fields, we find that the main magnetic properties of $FeWO_4$ nanostructures are the result of competitive phenomena between the inner planes ferromagnetism and an antiferromagnetic coupling between two successive planes having antiparallel alignment of spins. Our work offers an efficient route to gain further understanding of how to achieve shape-controlled synthesis of $FeWO_4$ nanocrystals with magnetic properties and may motivate potential applications of $FeWO_4$-based nanostructures.

Future works will focus on the search of new potentialities, such the analysis of electric properties from the experimental side, while, on the theoretical part, a clear area of improvement is to carry out a full optimization of the geometry for the different magnetic states at a more accurate and costly computational level, and it is currently under development.

Acknowledgments

The authors acknowledge the financial support of the Brazilian research financing institutions: FAPESP (No. 2009/53189-8/50303-4), CNPq and CAPES. This work is also supported by Generalitat Valenciana for *Prometeo*/2009/053 project, *Ministerio de Ciencia e Innovación* for project CTQ2009-14541-C02, Spanish MALTA-Consolider Ingenio 2010 Program (Project CSD2007-00045), Programa de Cooperación Científica con Iberoamerica

(Brasil), Ministerio de Educación (PHB2009-0065-PC). A. B. acknowledges a research grant from Generalitat Valenciana BEST/2011.

References

[1] Y. X. Zhou, H. B. Yao, Q. Zhang, J. Y. Gong, S. J. Liu, and S. H. Yu, Inorg. Chem. **48**, 1082 (2009).

[2] W. B. Hu, Y. M. Zhao, Z. L. Liu, C. W. Dunnill, D. H. Gregory, and Y. Q. Zhu, Chem. Mater. **20**, 5657 (2008).

[3] W. M. Qu, W. Wlodarski, and J. U. Meyer, Sensors and Actuators B **64**, 76 (2000).

[4] V. Felea, P. Lemmens, S. Yasin, S. Zherlitsyn, K. Y. Choi, C. T. Lin, and C. Payen, J. Phys.-Condens. Matt. **23**, 216001 (2011); H. Nojiri, S. Yoshii, M. Yasui, K. Okada, M. Matsuda, J. S. Jung, T. Kimura, L. Santodonato, G. E. Granroth, K. A. Ross, J. P. Carlo, and B. D. Gaulin, Phys. Rev. Lett. **106**, 237202 (2011); F. Ye, R. S. Fishman, J. A. Fernandez-Baca, A. A. Podlesnyak, G. Ehlers, H. A. Mook, Y. Q. Wang, B. Lorenz, and C. W. Chu, Phys. Rev. B **83**, 140401 (2011).

[5] S. H. Yu, B. Liu, M. S. Mo, J. H. Huang, X. M. Liu, and Y. T. Qian, Adv. Funct. Mater. **13**, 639 (2003).

[6] Y. X. Zhou, Q. Zhang, J. Y. Gong, and S. H. Yu, J. Phys. Chem. C **112**, 13383 (2008).

[7] J. Zhang, Y. Wang, S. K. Li, X. F. Wang, F. Z. Huang, A. J. Xie, and Y. H. Shen, CrystEngComm **13**, 5744 (2011).

[8] N. Stüβer, Y. Ding, M. Hofmann, M. Reehuis, B. Ouladdiaf, G. Ehlers, D. Gunther, M. Meiβner, and M. Steiner, J. Phys.: Condens. Matter **13**, 2753 (2001).

[9] S. Rajagopal, V. L. Bekenev, D. Nataraj, D. Mangalaraj, and O. Y. Khyzhun, J. Alloys Compd. **496**, 61 (2010).

[10] C. P. Landee and E. F. Westrum, J. Chem. Thermodyn. **8**, 471 (1976).

[11] S. Rajagopal, D. Nataraj, O. Y. Khyzhun, Y. Djaoued, J. Robichaud, and D. Mangalaraj, J. Alloys Compd. **493**, 340 (2010).

[12] E. Schmidbauer, U. Schanz, and F. J. Yu, J.Phys.-Condens. Matter. **3**, 5341 (1991).

[13] F. J. Yu, U. Schanz, and E. Schmidbauer, J. Cryst. Growth **132**, 606 (1993).

[14] I. Bilecka and M. Niederberger, Nanoscale **2**, 1358 (2010); W. Schumacher, A. Nagy, W. J. Waldman, and P. K. Dutta, J. Phys. Chem. C **113**, 12132 (2009); A. L. Washington and G. F. Strouse, J. Am. Chem. Soc. **130**, 8916 (2008). M. Baghbanzadeh, L. Carbone, P. D. Cozzoli, and C. O. Kappe, Angew. Chem. Int. Ed. **50**, 11312 (2011).

[15] V. M. Longo, L. Gracia, D. G. Stroppa, L. S. Cavalcante, M. Orlandi, A. J. Ramirez, E. R. Leite, J. Andrés, A. Beltrán, J. A. Varela, and E. Longo, J. Phys. Chem. C **115**, 20113 (2011); M. L. Moreira, J. Andrés, V. R. Mastelaro, J. A. Varela, and E. Longo, CrystEngComm **13**, 5818 (2011); D. P. Volanti, A. G. Sato, M. O. Orlandi, J. M. C. Bueno, E. Longo, and J. Andres, ChemCatChem **3**, 839 (2011).

[16] A. C. Larson and R. B. Von Dreele, *General Structure Analysis System (GSAS)* (Alamos National Laboratory Report, 2004), p.86.

[17] C. Escobar, Ciddresd.H, P. Kittl, and I. Dumler, Am. Miner. **56**, 489 (1971).

[18] R. Dovesi, V. R. Saunders, C. Roetti, R. Orlando, C. M. Zicovich-Wilson, B. Civalleri, F. Pascale, K. Doll, N. M. Harrison, I. J. Bush, P. D. Arco, and M. Llunell, CRYSTAL 09 Program (University of Torino Torino, 2009).

[20] CRYSTAL Basis Sets Library http://www.crystal.unito.it/Basis_Sets/Ptable.html.

[21] A. D. Walkingshaw, N. A. Spaldin, and E. Artacho, Phys. Rev. B **70**, 165110 (2004).

Table 1: Results of Rietveld refinement of $FeWO_4$ sample. Monoclinic symmetry, space group P_12/c_1.

Lattice parameters					
a (Å)	b (Å)	c (Å)	α (°)	β (°)	γ (°)
4.680	5.697(5)	4.984(1)	90.00	89.88	90.00
V(Å^3)	ρ (g/cm^3)				
132.90	7.589				
R_w = 10.32%; R_{wnb} = 8.23%; R_b = 7.79%; R_{exp} = 8.22% and σ = 1.26					
Atomic positions					
Atom	x	y	z	Occupancy	Multiplicity
Fe (2f)	0.500(0)	0.669(1)	0.250(0)	1	2
W (2e)	0.000(0)	0.176(5)	0.250(0)	1	2
O1 (4g)	0.226(5)	0.145(4)	0.581(6)	1	4
O2 (4g)	0.272(1)	0.352(6)	0.143(6)	1	4

FIGURES:

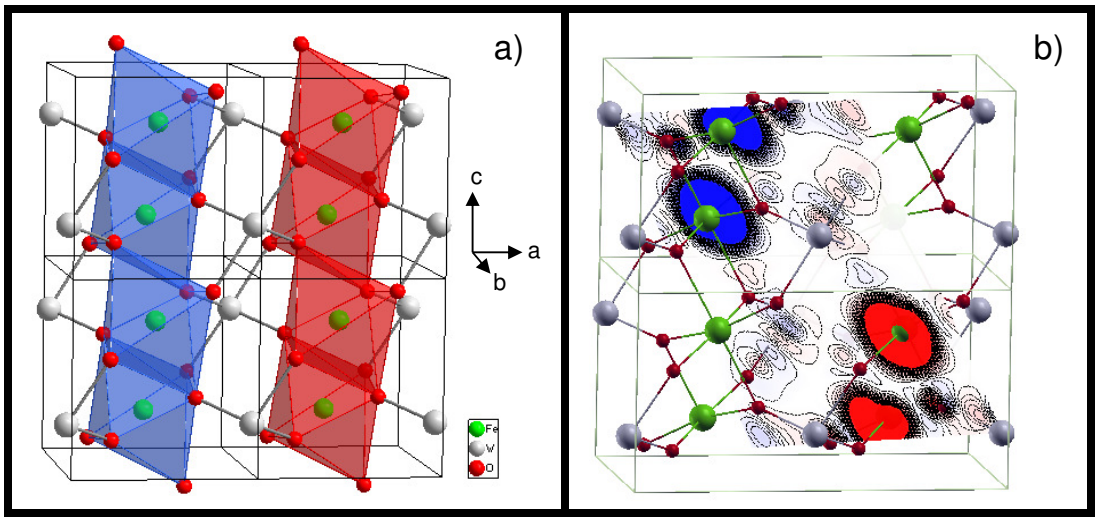

Figure 1: (a) Schematic representation of four monoclinic $FeWO_4$ unit cells illustrating the distorted octahedral (FeO_6) clusters. Frames indicate the crystallographic unit cells. (b) Spin distribution around Fe in two $FeWO_4$ magnetic unit cells. The red and the blue isolines represent the density of the alpha and beta spin, respectively.

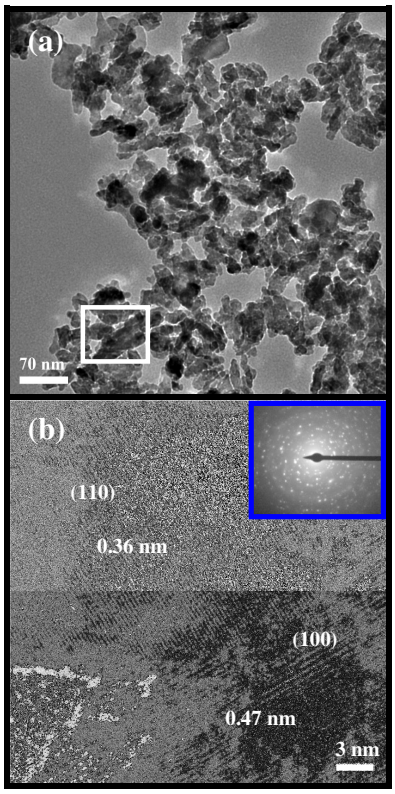

Figure 2: a) TEM images of the $FeWO_4$ nanocrystals. Inset is a SAED pattern; (b) HRTEM image of nanocrystals.

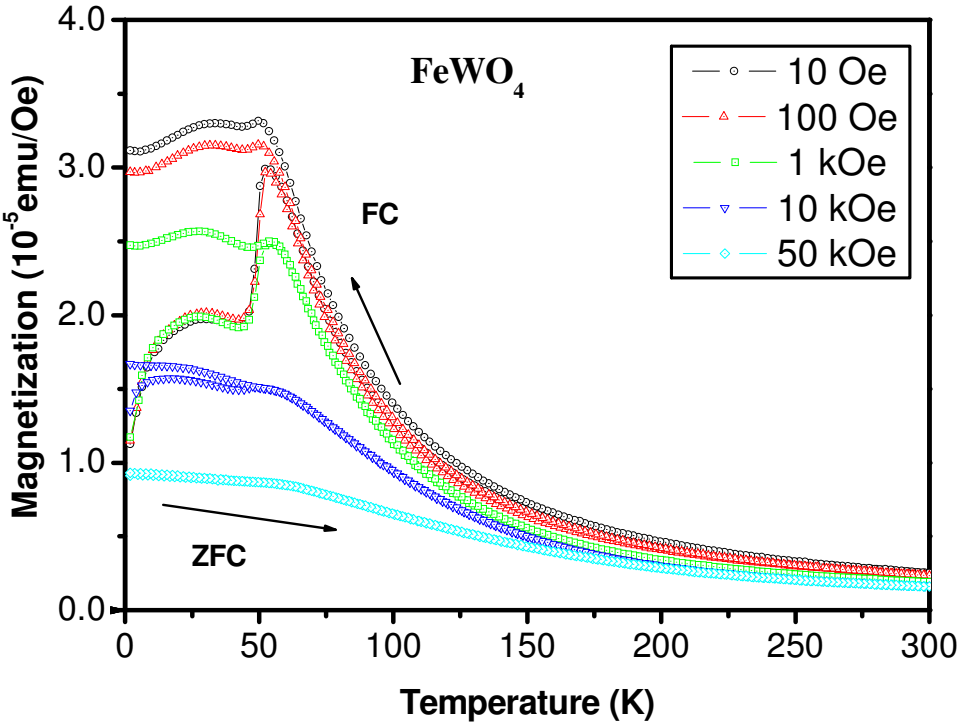

Figure 3: Temperature dependence of the ZFC and FC magnetizations for $FeWO_4$, measured under various applied fields.